nature nanotechnology

LETTERS

PUBLISHED ONLINE: 3 JULY 2011 | DOI: 10.1038/NNANO.2011.98

Thick lead-free ferroelectric films with high Curie temperatures through nanocomposite-induced strain

Sophie A. Harrington[1]*, Junyi Zhai[2], Sava Denev[3], Venkatraman Gopalan[3], Haiyan Wang[4], Zhenxing Bi[4], Simon A. T. Redfern[5], Seung-Hyub Baek[6], Chung W. Bark[6], Chang-Beom Eom[6], Quanxi Jia[2], Mary E. Vickers[1] and Judith L. MacManus-Driscoll[1]

Ferroelectric materials are used in applications ranging from energy harvesting to high-power electronic transducers[1]. However, industry-standard ferroelectric materials contain lead, which is toxic and environmentally unfriendly[2]. The preferred alternative, $BaTiO_3$, is non-toxic and has excellent ferroelectric properties, but its Curie temperature of ~130 °C is too low to be practical[3]. Strain has been used to enhance the Curie temperature of $BaTiO_3$ (ref. 4) and $SrTiO_3$ (ref. 5) films, but only for thicknesses of tens of nanometres, which is not thick enough for many device applications. Here, we increase the Curie temperature of micrometre-thick films of $BaTiO_3$ to at least 330 °C, and the tetragonal-to-cubic structural transition temperature to beyond 800 °C, by interspersing stiff, self-assembled vertical columns of Sm_2O_3 throughout the film thickness. The columns, which are 10 nm in diameter, strain the $BaTiO_3$ matrix by 2.35%, forcing it to maintain its tetragonal structure and resulting in the highest $BaTiO_3$ transition temperatures so far.

Many ferroelectric systems are being studied as replacements for $PbZr_xTi_{(1-x)}O_3$, with bismuth layered compounds[6] being a popular subject of investigation. Although the T_c for these materials can be high, up to 790 °C, property optimization is difficult due to the need for careful textural alignment. $BiFeO_3$ and other titanate perovskites are alternative high-T_C ferroelectrics; however, their processing windows are narrow, and doping needs to be extremely precise[7–9]. Haeni *et al.*[5] first demonstrated the enhancement of T_c in $SrTiO_3$ thin films by making use of substrate-induced epitaxial strain, with Choi *et al.* demonstrating the same in $BaTiO_3$ films[4]. However, because of strain relaxation through the thickness of these films, increasing T_c by means of substrate control is limited to films that are only tens of nanometres thick[10,11], which is impractical, because many ferroelectric devices require much thicker films.

A novel method to provide strain control in much thicker films involves the growth of vertical nanocomposites[12–16]. In $BiFeO_3$:Sm_2O_3 (ref. 17), high compressive vertical strain levels of ~1.5% have been demonstrated, with a strong improvement in dielectric properties and reduced leakage[18]. Here, we demonstrate a nanocomposite system of $BaTiO_3$:Sm_2O_3 that generates out-of-plane tension in the $BaTiO_3$ (BTO) of ~2.35%. Sm_2O_3 (SmO) is the ideal strain controlling second phase because it substitutes only minimally into the BTO, it has a large elastic modulus (125 GPa, compared to 67 GPa for BTO) and is insulating[19,20]. In >1-μm-thick films, a strong increase in the tetragonal to cubic phase transition temperature, from 130 °C to >800 °C, and concomitant increase in Curie temperature are demonstrated. Such enhancements in thick films have opened a new approach to using BTO in high-temperature ferroelectric applications.

Films were grown using pulsed laser deposition (from a single target containing a 50:50 mix of BTO and SmO) onto (001) Nb-doped $SrTiO_3$ substrates at 800 °C. Figure 1 presents cross-sectional transmission electron microscopy (TEM) images of 600-nm-thick composite films, showing self-assembled SmO nanocolumns with diameters of ~10 nm, which are evenly sized and distributed, embedded in a BTO matrix. The nanocolumns extend perpendicular to the substrate through the entire thickness of the film (Fig. 1a,c). The composite nanostructure arises from a process of nucleation and growth, with small, cylindrical pillars forming (Fig. 1b) to allow the surface energy of the BTO matrix to be minimized[21]. This nanostructure is similar to that of $BaTiO_3$:$CoFe_2O_4$ composites[22], except that it is the lower compliance $CoFe_2O_4$ rods that adapts to accommodate the mismatch strain (−0.8% out-of-plane); here, critically, it is the BTO matrix that is the lower compliance phase and therefore becomes strained (+2.35% out-of-plane).

From X-ray scans, the in-plane orientation for BTO was found to be $\langle 100\rangle_{BTO} \parallel \langle 100\rangle_{STO}$ and for the SmO $\langle 100\rangle_{SmO} \parallel \langle 110\rangle_{STO}$. Table 1 presents the room-temperature lattice parameters. It is found that $2 \times (001)_{BTO\text{-strained-comp.}}$ ($= 2 \times 4.078$ Å $= 8.16$ Å) $\approx$ $3 \times (004)_{SmO\text{-strained-comp.}}$ ($= 3 \times 10.913/4$ Å $= 8.18$ Å). A schematic of the crystallographic matching of the two phases consistent with these calculations is represented in Fig. 1d. The cell volume for the strained BTO is 65.8 Å^3, which is close to that of bulk BTO (64.4 Å^3), indicating minimal chemical modification of the BTO by the SmO. This was further confirmed by energy-dispersive X-ray spectroscopy (EDX) on individual crystals of BTO that had been reacted with SmO at 1,200 °C for 2 days.

Reciprocal space maps about the $(\bar{1}\bar{1}3)$ STO substrate reveal a clear shift in the position of the $(\bar{1}\bar{1}3)$ BTO peak from the pure film to the composite film (Fig. 2a,b). The pure BTO film is fully relaxed, as expected for this thickness of film (1 μm). The $(\bar{1}\bar{1}3)$ pure BTO peak is broad, indicating a spread of lattice parameters, as is expected for a film that has gradual relaxation with increasing

[1]Department of Materials Science, University of Cambridge, Cambridge, CB2 3QZ, UK, [2]Center for Integrated Nanotechnologies, MS K771, Los Alamos National Laboratory, Los Alamos, New Mexico 87545, USA, [3]Department of Materials Science and Engineering, Pennsylvania State University, University Park, Pennsylvania, USA, [4]Department of Electrical and Computer Engineering, Texas A and M University, 3128 TAMU, College Station, Texas 778433128, USA, [5]Department of Earth Sciences, University of Cambridge, Cambridge CB2 3EQ, UK, [6]Department of Materials Science and Engineering, University of Wisconsin-Madison, Madison, 53706, Wisconsin, USA. *e-mail: sah59@cam.ac.uk

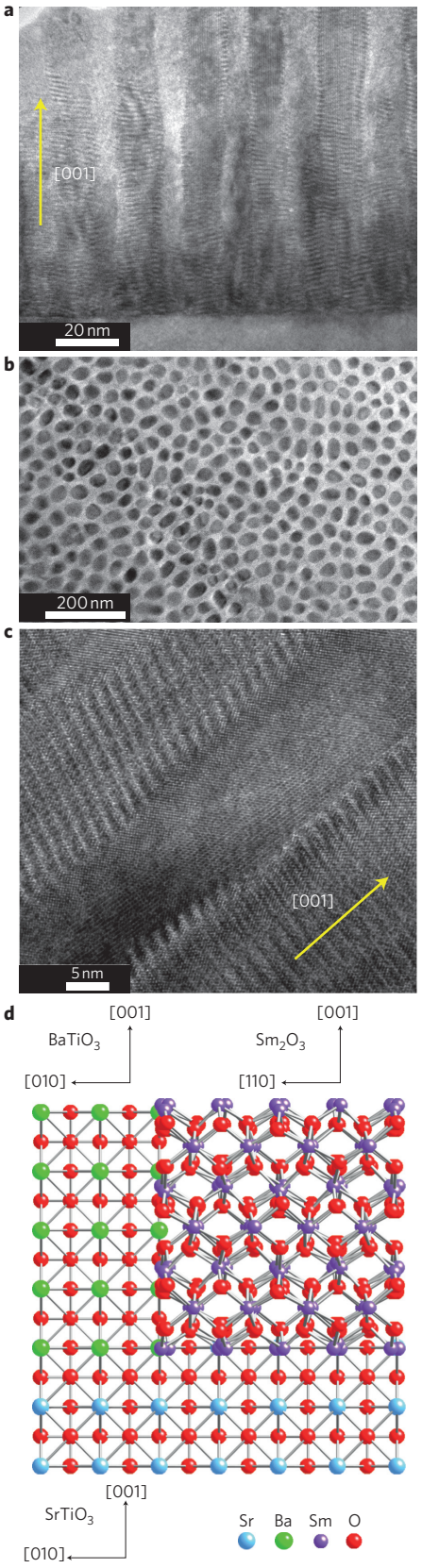

Figure 1 | Self-assembled vertical nanostructure. a–c, TEM images of a 600-nm-thick $BaTiO_3$:Sm_2O_3 film on $SrTiO_3$: cross-section (**a**) near the film–substrate interface; plan view (**b**); cross-section (**c**) revealing structure still present near the film-free surface. Sm_2O_3 shows a darker contrast compared with $BaTiO_3$. Yellow arrow represents *c*-axis direction. **d**, Crystallographic model of interface matching.

Table 1 | Lattice parameters of 1-μm-thick films.

	Out-of-plane lattice parameter (Å)	In-plane lattice parameter (Å)
$SrTiO_3$ substrate (JCPDS # 35-0734)	3.9050	3.9050
$BaTiO_3$ bulk[33]	4.0343(5)	3.9939(5)
Sm_2O_3 bulk (JCPDS # 15-0813)	10.928*	10.928
Pure $BaTiO_3$ film	3.984(3)	4.041(5)
Pure Sm_2O_3 film	10.822(3)	11.014(5)
$BaTiO_3$ in composite	4.078(3)	4.016(5)

*a (Sm_2O_3)/4 × $\sqrt{2}$ ≈ a (STO).

thickness. The $(\bar{1}\bar{1}3)$ BTO peak in the composite is shifted away from the $(\bar{1}\bar{1}3)$ STO peak (Fig. 2b) and towards the $(\bar{4}08)$ SmO peak, which shows both a lack of film relaxation and, more significantly, strain control by the SmO phase and not by the STO substrate. Also, the $(\bar{1}\bar{1}3)$ BTO peak is much sharper than in the pure film, indicating little spread of the lattice parameters and hence little or no strain relaxation through the thickness of the film. For the BTO in the composite, the shift corresponds to an extension out-of-plane of +2.35% with respect to the pure BTO film (+1.07% with respect to bulk BTO) and a compression in-plane of –0.62% with respect to the pure BTO film. These levels of strain are sufficient from theoretical predictions to produce an increase in the transition temperature to the ~700–800 °C values measured here; the precise predicted value, however, depends on the particular model adopted[4,23]. The stiffer SmO was only slightly compressed out-of-plane, as expected from its higher compliance compared to BTO.

Figure 2c shows the dependence of the *a* and *c* lattice parameters with temperature. For pure BTO bulk, the tetragonal to cubic phase transition is observed at 130 °C, as expected. For a 150-nm-thick composite film, the transition is in line with theoretical predictions for the level of strain in the film (~800 °C), whereas for a 600 nm film, at the highest possible measurement temperature of 800 °C, the transition has not yet taken place. The volume of the substrate-strained region is proportionally much less in the thicker film, allowing vertical strain to dominate the net behaviour and increase T_c by such a marked amount. A comparative 50 nm pure BTO film controlled by a highly mismatched substrate, with the highest previously reported transition of ~560 °C (ref. 4) is shown for reference. The 800 °C transition in this work is the highest transition temperature yet recorded in BTO; furthermore, this is achieved in micrometre-thick films.

Optical second harmonic generation (SHG) signals are plotted versus temperature for two composite samples in Fig. 2d. The dominant electric dipole contribution to optical SHG is exhibited only by materials that lack inversion symmetry. Because ferroelectrics lack inversion symmetry, the presence of SHG suggests a polar structure. There is no SHG signal in normal incidence for either sample, which is expected for out-of-plane polarization. However, for a finite angle of incidence at 45°, BTO produces an SHG signal. For the 1.25-μm-thick film, the transition temperature has increased to ~320 °C, below which long-range polar order sets in. Local polar order (without long-range correlation) continues up to ~700–800 °C, as indicated by a weak SHG signal and the inset polar plot. Analysis of the SHG polar plots suggests tetragonal symmetry with 4*mm* point group symmetry (equation 1), even at 795 °C (Fig. 2d, inset).

The thinner 600 nm film exhibits a diffuse transition in SHG, suggesting an inhomogeneous distribution of stress, consistent with some contribution of substrate strain control in material at the base of the film. Atomic displacement and field-switchable spontaneous polarization (that is, ferroelectricity) are two physically

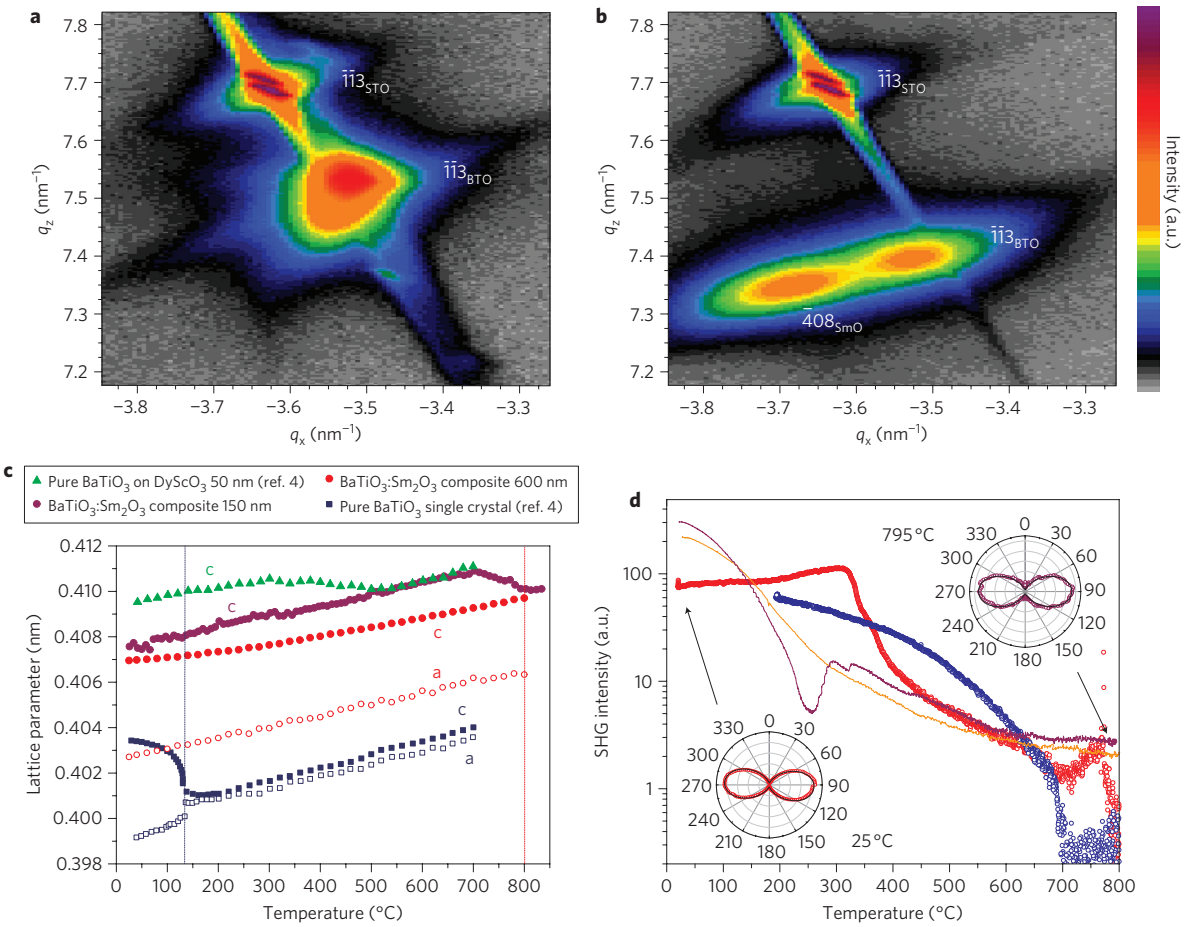

Figure 2 | Enhanced tetragonality at elevated temperature. a,**b**, X-ray reciprocal space maps about the ($\bar{1}\bar{1}3$) of the STO substrate for a pure BTO film (**a**) and a composite film (**b**), both with a thickness of 1 μm. **c**, Temperature dependence of lattice parameters comparing a single crystal and a substrate-controlled pure BTO film (50 nm) (reproduced from ref. 4) with BTO:SmO composite films (150 and 600 nm). Closed symbols: out-of plane lattice parameter calculated from the (002) X-ray peak; open symbols: in-plane lattice parameter calculated from the (101) X-ray peak. **d**, Dependence of SHG signal on temperature for a 600 nm film (purple, heating; orange, cooling) and a 1.25 μm film (red, heating; blue, cooling). Inset: SHG signal (radial distance) versus fundamental polarization (azimuthal angle) at room temperature (25 °C) and 795 °C for *p* (signal polarized in the incidence plane). Black lines are a fit from equation (1) (see Methods).

separate things, detected by different experiments[24], so direct electrical measurements were also necessary.

The dielectric constant as a function of frequency and temperature was measured for both pure and composite films (shown at 10, 25, 50 and 100 kHz in Fig. 3, upper inset), and in several composite samples a sharp dielectric peak was measured between ~700 °C and ~800 °C, without a clear dependence of peak temperature on thickness, but broadly consistent with the range of structural transition temperatures measured by X-ray. We observe a peak at 700 °C for a 1-μm-thick film; there was no shift in this peak position with frequency, indicating a normal, rather than diffuse, phase transition[25]. The peak dielectric constant value was ~7,000. The sharpness of the peak, its frequency invariance and its temperature coincident to the X-ray transition together indicate that a transition from tetragonal to cubic structures is being measured. The pure 1-μm-thick reference film shows a broad peak at over 100 °C and a peak value of ~2,000. The data are typical for a thick pure BTO film[26–29] where there is a partial relaxation of lattice parameters, as was seen in the reciprocal space map of the reference film (Fig. 2a).

From ferroelectric hysteresis measurements, a 1 μm composite film was confirmed to be ferroelectric to at least 330 °C (Fig. 3). A non-decreasing remanent polarization (P_r) of 21 μC cm^{-2} (calculated using the area of the BTO component of the film) was recorded both at room temperature and at 330 °C. The value is similar to that from our pure BTO films, and those from the literature[30], measured at room temperature. The non-square hysteresis behaviour and high coercive field ($E_c \approx 200$ kV cm^{-1}) compared to bulk material ($E_c \approx 1$ kV cm^{-1}; ref. 31) can be explained by the pinning of the ferroelectric/ferroelastic domain walls by the SmO phase. The shift of the loops to the left is caused by the use of different top and bottom electrodes, and the increased area of loop with increasing temperature arises from increased leakage. Because strong polarization is achieved in the BTO matrix with dimensions of only 10 nm, but in free-standing nanowires of similar diameter it is degraded[32], it is clear that strain coupling to SmO prevents the BTO from undergoing deleterious surface reconstruction and allows for a stable nanoscale ferroelectric.

The leakage current was reduced (Fig. 3, lower inset) to 2.2×10^{-7} A cm^{-2} from 3.3×10^{-6} A cm^{-2} (at 200 kV cm^{-1}) for an equivalent pure BTO film. This is consistent with the observations of higher crystalline quality and higher Curie temperature of the BTO in the composite. Both the asymmetry and magnitude of the leakage data are in agreement with the literature[30].

In summary, self-assembled nanoscale composites of BTO and SmO (up to 1.25 μm thick) were grown that exhibited tetragonality up to at least 800 °C (potential for ferroelectricity up to this temperature) and strong remanent polarization to at least 330 °C. The enhanced T_c is a consequence of uniform, vertical

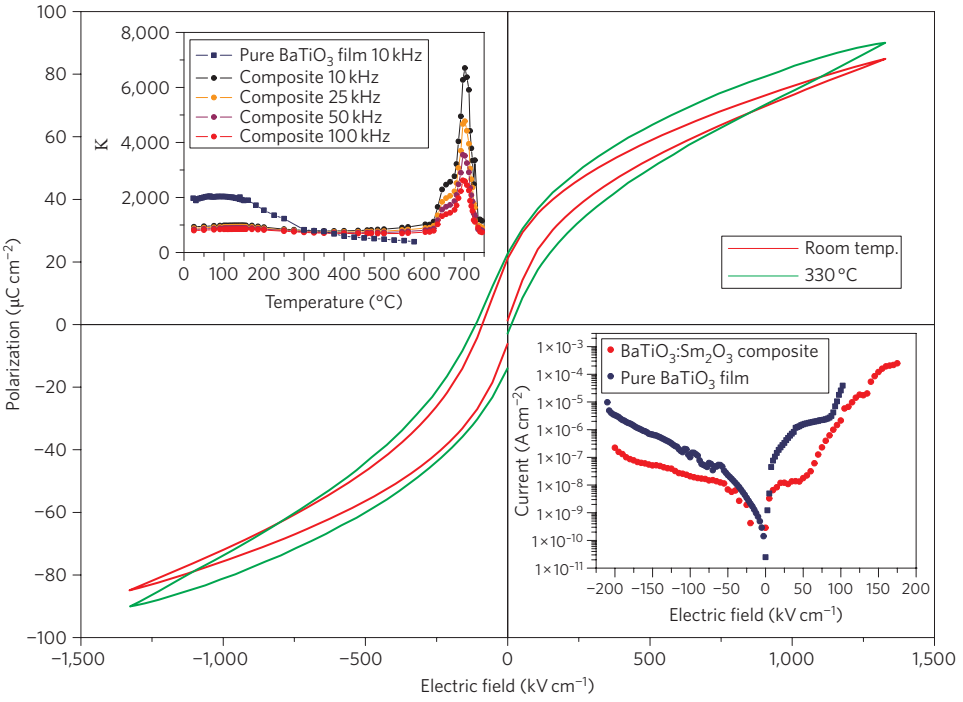

Figure 3 | Direct electrical measurements. Polarization versus electric field hysteresis loops of 1 μm BTO:SmO thin-film capacitors at room temperature and 330 °C. Upper inset: dependence of dielectric constant on temperature for pure and composite films with a thickness of 1 μm, at 10, 25, 50 and 100 kHz. Lower inset: leakage current as a function of applied field for the same thickness (600 nm) of pure BTO and BTO:SmO thin films. The Pt top electrode was positively biased.

strain coupling between stiff 10 nm regular interspersed nanocolumns of SmO and a surrounding BTO nanomatrix, preventing the onset of the tetragonal to cubic phase transition. The nanocomposite structure improved BTO crystalline quality and reduced the leakage current.

Methods

Pure BTO and BTO:SmO 50:50 composite films were grown onto (001) 1.4 at% Nb-doped $SrTiO_3$ substrates at 800 °C in 0.2 mbar of oxygen, by pulsed laser deposition using a KrF laser ($\lambda = 248$ nm) with a fluence of 2 J cm^{-2} and a repetition rate of 1 Hz. Film thicknesses in the range 50 nm to 1.25 μm were deposited. TEM was performed on a JEOL 2011FEG/JEOL 4000EX/Philips CM30 microscope. X-ray diffraction was carried out with a Bruker D8 diffractometer using CuKα radiation. Reciprocal space maps were collected about the $(\bar{1}03)$ and $(\bar{1}\bar{1}3)$ of STO and precise peak positions were obtained from asymmetric line scans made across the regions of interest, in combination with profile fitting. Diffraction patterns were obtained *in situ* at high temperature by rapid scans over the (002) (*a* lattice parameter) and skew symmetric scans for the (101) peak (*c* lattice parameters) such that the sample was held at each temperature for no more than 5 min, with temperature steps varying between 5 and 20 °C. SHG measurements were carried out at a laser wavelength of 800 nm, with 65 fs laser pulses incident on the substrate side of the sample at an angle of 45°. The expected intensities of the SHG signal polarized in the incidence plane (p) and perpendicular to the incidence plane (s) are given by

$$I_p^{2\omega} = A(B\cos^2\theta + \sin^2\theta)^2 \quad (1)$$

$$I_s^{2\omega} = C\sin^2 2\theta \quad (2)$$

where θ is the angle of the input polarization measured from the plane of incidence, and A, B and C are coefficients that depend on the nonlinear optical coefficients of BTO, indices of refraction and angle of incidence. Pt electrodes ($\sim 3 \times 10^{-8}$ m^2) were sputtered onto the film surface, and electrical measurements were carried out using a Radiant 100 precision ferroelectric tester and HP4942A impedance analyser. The dielectric constant was measured with frequency, and its dependence on temperature extracted at 10, 25 and 50 kHz with a 50 mV field. Hysteresis loops were recorded at 1 kHz.

Received 28 April 2011; accepted 24 May 2011; published online 3 July 2011

References

1. Haertling, G. H. Ferroelectric ceramics: history and technology. *J. Am. Ceram. Soc.* **82,** 797–818 (1999).
2. Maeder, M. D., Damjanovic, D. & Setter, N. Lead free piezoelectric materials. *J. Electroceramics* **13,** 385–392 (2004).
3. Takenaka, T. & Nagata, H. Current status and prospects of lead-free piezoelectric ceramics. *J. Eur. Ceram. Soc.* **25,** 2693–2700 (2005).
4. Choi, K. J. *et al.* Enhancement of ferroelectricity in strained $BaTiO_3$ thin films. *Science* **306,** 1005–1009 (2004).
5. Haeni, J. H. *et al.* Room-temperature ferroelectricity in strained $SrTiO_3$. *Nature* **430,** 758–761 (2004).
6. Wang, H. & Ren, M. Synthesis and ferroelectric properties of $SrBi_2Ta_2O_9$/$Bi_4Ti_3O_{12}$/p-Si multilayer thin films by sol–gel. *J. Mater. Sci. Mater. Electron.* **17,** 165–169 (2006).
7. Qi, X. D., Dho, J., Tomov, R., Blamire, M. G. & MacManus-Driscoll, J. L. Greatly reduced leakage current and conduction mechanism in aliovalent-ion-doped $BiFeO_3$. *Appl. Phys. Lett.* **86,** 062903 (2005).
8. Takenaka, T., Nagata, H., Hiruma, Y., Yoshii, Y. & Matumoto, K. Lead-free piezoelectric ceramics based on perovskite structures. *J. Electroceram.* **19,** 259–265 (2007).
9. Gomah-Pettry, J. R., Saïd, S., Marchet, P. & Mercurio, J. P. Sodium-bismuth titanate based lead-free ferroelectric materials. *J. Eur. Ceram. Soc.* **24,** 1165–1169 (2004).
10. Wimbush, S. C. *et al.* Interfacial strain-induced oxygen disorder as the cause of enhanced critical current density in superconducting thin films. *Adv. Funct. Mater.* **19,** 835–841 (2009).
11. Nagarajan, V. *et al.* Misfit dislocations in nanoscale ferroelectric heterostructures. *Appl. Phys. Lett.* **86,** 192910 (2005).
12. Moshnyaga, V. *et al.* Structural phase transition at the percolation threshold in epitaxial $(La_{0.7}Ca_{0.3}MnO_3)_{1-x}$:$(MgO)_x$ nanocomposite films. *Nature Mater.* **2,** 247–252 (2003).
13. Macmanus-Driscoll, J. L. *et al.* Strongly enhanced current densities in superconducting coated conductors of $YBa_2Cu_3O_{7-x}$+$BaZrO_3$. *Nature Mater.* **3,** 439–443 (2004).
14. Aggarwal, S. *et al.* Spontaneous ordering of oxide nanostructures. *Science.* **287,** 2235–2237 (2000).
15. Zavaliche, F. *et al.* Electric field-induced magnetization switching in epitaxial columnar nanostructures. *Nano Lett.* **5,** 1793–1796 (2005).
16. Fouchet, A. *et al.* Spontaneous ordering, strain control, and multifunctionality in vertical nancomposite heteroepitaxial films. *IEEE Trans. Ultrason. Ferr.* **56,** 1534–1538 (2009).

17. MacManus-Driscoll, J. L. *et al.* Strain control and spontaneous phase ordering in vertical nanocomposite heteroepitaxial thin films. *Nature Mater.* **7,** 314–320 (2008).
18. Yang, H. *et al.* Vertical interface effect on the physical properties of self-assembled nanocomposite epitaxial films. *Adv. Mater.* **21,** 3794–3798 (2009).
19. Munro, R. G. *Elastic Moduli Data for Polycrystalline Ceramics* 6853 (NISTIR, 2002).
20. IEEE. *Proceedings of the 5th International Symposium on Micro Machine and Human Science* 75 (Nagoya, 1994).
21. MacManus-Driscoll, J. L. Self-assembled heteroepitaxial oxide nanocomposite thin film structures: designing interface-induced functionality in electronic materials. *Adv. Funct. Mater.* **20,** 2035–2045 (2010).
22. Zheng, H. *et al.* Multiferroic $BaTiO_3$-$CoFe_2O_4$ nanostructures. *Science* **303,** 661–663 (2004).
23. Schlom, D. G. *et al.* Strain tuning of ferroelectric thin films. *Annu. Rev. Mater. Res.* **37,** 589–626 (2007).
24. Megaw, H. D. Origin of ferroelectricity in barium titanate and other perovskite-type crystals. *Acta Cryst.* **5,** 739–749 (1952).
25. Kuwabara, M., Goda, K. & Oshima, K. Coexistence of normal and diffuse ferroelectric-paraelectric phase transitions in (Pb,La)TiO_3 ceramics. *Phys. Rev. B.* **42,** 10012–10015 (1990).
26. Shintani, Y. & Tada, O. Preparation of thin $BaTiO_3$ films by DC diode sputtering. *J. Appl. Phys.* **41,** 2376–2380 (1970).
27. Iijima, K., Terashima, T., Yamamoto, K., Hirata, K. & Bando, Y. Preparation of ferroelectric $BaTiO_3$ thin-films by activated reactive evaporation. *Appl. Phys. Lett.* **56,** 527–529 (1990).
28. Yoneda, Y. *et al.* Ferroelectric phase-transition in $BaTiO_3$ films. *J. Phys. Soc. Jpn* **62,** 1840–1843 (1993).
29. Nose, T., Kim, H. T. & Uwe, H. Dielectric property of epitaxial-films of $BaTiO_3$ synthesized by laser-ablation. *Jpn J. Appl. Phys. 1* **33,** 5259–5261 (1994).
30. Abe, K., Komatsu, S., Yanase, N., Sano, K. & Kawakubo, T. Asymmetric ferroelectricity and anomalous current conduction in heteroepitaxial $BaTiO_3$ films. *Jpn. J. Appl. Phys.* **36,** 5846–5853 (1997).
31. Jaffe, B., Cook, W. R. Jr & Jaffe, H. *Piezoelectric Ceramics* (Academic, 1971).
32. Hong, J. W. & Fang, D. N. Size-dependent ferroelectric behaviours of $BaTiO_3$ nanowires. *Appl. Phys. Lett.* **92,** 012906 (2008).
33. Megaw, H. D. Crystal structure of barium titanate. *Nature* **155,** 484–485 (1945).

Acknowledgements

The authors are grateful to A. Fouchet for his assistance with preliminary studies. The work was supported by Downing College Cambridge, the European Commission (Marie Curie Excellence Grant 'NanoFen', MEXT-CT-2004-014156), European Research Council (ERC) (grant no. ERC-2009-adG 247276), UK Engineering and Physical Sciences Research Council and US National Science Foundation (NSF 07-09831 and ECCS-0708759). We wish to acknowledge the use of the Chemical Database Service at Daresbury and help from the US Department of Energy through the Los Alamos National Laboratory/ Laboratory Directed Research and Development programme and the Center for Integrated Nanotechnologies.

Author contributions

H.W. and Z.B. collected and analysed TEM images. V.G. and S.D. were responsible for SHG data. C.B.E., S.A.T.R., S.H.B. and C.W.B. were responsible for high-temperature XRD measurements. J.Z. advised on direct electrical measurements. M.E.V. and Q.J. discussed the results and commented on the manuscript. S.A.H. prepared films, collected room-temperature XRD data, performed direct electrical measurements and analysed data. S.A.H. and J.L.M. co-wrote the manuscript.

Additional information

The authors declare no competing financial interests. Supplementary information accompanies this paper at www.nature.com/naturenanotechnology. Reprints and permission information is available online at http://www.nature.com/reprints. Correspondence and requests for materials should be addressed to S.A.H.